

The mid-infrared spectrum of the transiting exoplanet HD 209458b

M.R. Swain¹, J. Bouwman², R. Akeson³, S. Lawler³, & C. Beichman³

ABSTRACT

We report the spectroscopic detection of mid-infrared emission from the transiting exoplanet HD 209458b. Using archive data taken with the Spitzer/IRS instrument, we have determined the spectrum of HD 209458b between 8.25 and 13.25 μm with an average SNR of ~ 4 in each 0.25 μm spectral channel. We have used two independent methods to determine the planet spectrum and find the results are in good agreement. In the mid-infrared, the planet spectrum is dominated by thermal emission with a temperature consistent with previous estimates. The absence of strong spectral features is significant and is most consistent with emission at these wavelengths originating primarily from optically thick clouds located at relatively high elevation in the planet's atmosphere. This work required development of improved methods for Spitzer/IRS data calibration that increase the achievable dynamic range for observations of bright point sources.

Subject headings: planetary systems: hot Jovian exoplanet, techniques: infrared spectroscopy

1. Introduction

The Spitzer Space Telescope has revolutionised the observational characterization of exoplanets by detecting infrared emission from these objects; measurements have been reported for HD 209458b (Deming et al. 2004), TrES-1 (Charbonneau et al. 2005), HD 189733b

¹Jet Propulsion Laboratory, 4800 Oak Grove Drive, Pasadena, CA 91109

²Max-Planck Institute for Astronomy, Konigstuhl 17, D-69117 Heidelberg Germany

³Michelson Science Center, California Institute of Technology, MS 100-22, Pasadena, CA, 91125

(Deming et al. 2006), and *v* Andromeda b (Harrington et al. 2006). HD 209458b, the first reported transiting exoplanet (Charbonneau, et al. 2000), is located at a distance of 47 pc and has a G0 stellar primary ($V = 7.6$ mag). With an orbit of 3.52 days and a mass of $M_{planet} = (0.66 \pm 0.04)M_J$ (Wittenmmyer et al. 2005), HD 209458b is a member of the hot Jovian class of extra-solar planets. The radius of HD 209458b is $(1.35 \pm 0.07)R_J$, 10-20% larger than predicted by irradiated planet models (Wittenmmyer et al. 2005). The detection of infrared emission from hot Jovian exoplanets has stimulated extensive theoretical work on the atmospheric structure and emission of these planets. Constraining the model predictions for infrared emission from hot Jovian atmospheres is an important motivation for current observing programs. To date, constraints for theoretical analysis are based primarily on broad-band measurements of exoplanet emission.

Spectral characterisation of hot Jovian exoplanets is a high priority and is essential to distinguish between different atmospheric emission models. Spectroscopic detection of exoplanet emission has proved challenging from the ground (Richardson et al. 2003; Deming et al. 2005); space-based infrared spectroscopy is particularly appealing due to the absence of an atmosphere, improved signal-to-noise (SNR), and instrument stability. However, observations with the Spitzer IRS instrument are complicated by systematic errors that are large compared to the observable signature. Thus, calibrating the instrument’s systematic effects is essential. In this paper we present results based on a new approach for calibrating the major instrument systematic effects affecting these observations. Using data taken from the Spitzer archive, we report the detection of the spectral flux in HD 209458b using two semi-independent methods.

2. Observations

The observations we analyzed (originally proposed by J. Richardson and collaborators) were taken with the Spitzer Space Telescope (Werner et al. 2004) using the Infrared Spectrograph (IRS; Houck et al. 2004). The data were taken on 6 July 2005 and 13 July 2005 as two separate Astronomical Observing Requests (AORs 14817792 and 14818048) and provide approximately continuous coverage of the secondary eclipse event (see Fig. 1). The timing of the observations is well suited for application of the secondary eclipse technique (also termed “occultation spectroscopy”), in which data from portions of the orbit in which light originates from “star+planet” and “star” are differenced to obtain the planet’s emission (Richardson et al. 2003). For both sets of observations, the IRS instrument was operated in first order at low spectral resolution with a nod executed at the midpoint of the observations. Thus, there are two completely independent data sets that span an interval sufficient

to cover the sequence “star+planet”, ingress, “planet”, egress, “star+planet”. Each nod contains 140 samples with an integration time of 52 seconds each.

We use the ephemeris for HD 209458b (Wittenmmyer et al. 2005) and the measured light curve (Brown et al. 2001) to determine the correspondence between the observations and the orbital position of the exoplanet. In what follows, we will refer to the segment of the orbital phase when both star and planet are visible as “A”. Similarly, we refer to the segment of orbital phase when only the star is visible (when the planet is passing behind the star) as “B”. We have restricted our analysis to wavelengths between 8.25 and 13.25 μm to avoid known calibration uncertainties at the edges of the IRS instrument passband in this configuration.

3. Analysis

The initial extraction and calibration of these data is based on a modified version of the standard Spitzer/IRS pipeline (Bouwman et al. 2006). The extracted spectral flux time series suffers from three major effects that completely dominate (by a factor of ~ 10) the expected signature of secondary eclipse flux decrement of ~ 0.0025 (Deming et al. 2004). These effects are (i) a flux offset between nods, (ii) a periodic flux modulation, and (iii) monotonic flux drift within a nod (see Fig. 1). These temporal features are not random; to first order, they are wavelength independent, and a scatter diagram shows that the spectral flux values are highly correlated (correlation coefficients of ~ 0.99). We find that these three major effects are caused by errors in background subtraction and telescope pointing.

Background subtraction: In the mid-infrared, accurate measurement of the infrared source flux requires subtraction of the background due to local zodiacal emission. For the Spitzer IRS instrument, this is normally done by subtracting the measurement of the sky made at the nod 2 position from the nod 1 data and *vice-versa*. We used this approach for the observations of HD 209458b and found an offset in the background between nods 1 and 2; this is plausible since there could be structure in the background. However, inspection of IRS calibrator star data shows that the difference in the background between the nods is systematic in that it occurs for all the multiply observed sources we checked; the effect is highly repeatable, and is proportional to the measured source flux. IRS calibrators observed with a series of slit offsets show the measured source flux decreases with the slit offset from the target and the background offset is proportional to the measured flux. This suggests that some of the light from the source “leaks” into the background. Because the Spitzer PSF is asymmetric (Bayward & Burgarolas 2004), the leakage differs in nod 1 and nod 2. We have used observations of the IRS calibrator stars HR 6606 and HR 7341 to determine

the amount of a point source leakage into the background estimate. Between 8 and 13 μm , the correction we derive is $\sim 0.4\%$ for nod 1 and $\sim 0.9\%$ for nod 2. Applying the correction for source leakage into the background causes the background offset to vanish (see Fig. 2). For many observations, this correction is not necessary. However, for high dynamic range measurements on bright point sources, failure to correct the leakage of the source into the background estimate limits the dynamic range to $\sim 150:1$ and leaves significant systematic residuals for each nod. A more detailed explanation of the derivation and application of the background correction for source leakage will be described in a forthcoming paper. In our data reduction, we applied the correction for source leakage in the estimate of the background; the background-subtracted source data were then analyzed in two different ways to determine the planet spectrum.

Method 1 - Spectral Flat Field: This approach begins with the assumption that changes in the measured flux have a wavelength-independent component, characterised by $G(t)$, which can vary on a time scale of minutes, and a wavelength-dependent component, $G(\lambda)$, which is stable for a given nod but can change between nods. The $G(\lambda)$ term is removed by construction of a spectral flat. We derived a spectral flat for each nod by comparing the average flux in each spectral channel to the flux, $F(\lambda)$, of a stellar photosphere model for HD 209458 (Kurucz 1992) normalized to the 12 μm flux. Thus at each wavelength, λ , the spectral flat is defined as the inverse of $[S_B(\lambda)/F_{Kurucz}(\lambda)] \times [F_{Kurucz}(12)/S_B(12)]$ where S_B is the measured flux observed in interval B. After normalization of each nod by the associated spectral flat field, the data are assumed to vary only in time; a more extensive discussion of this technique can be found in Bryden et al. (2006) and Beichman et al. (2006). To reject the wavelength-independent $G(t)$ term, we constructed a differential observable using the following method. During period A (star+planet), the measured flux, $S_A(\lambda)$, at can be written as,

$$S_A(\lambda) = G(t)F_*(\lambda) \left[1 + \frac{F_p(\lambda)}{F_p(\lambda')} \frac{F_p(\lambda')}{F_*(\lambda')} \frac{F_*(\lambda')}{F_*(\lambda)} \right], \quad (1)$$

where $F(\lambda)$ is the true source flux, with the subscripts referring to the star or planet, and λ' is a reference wavelength selected for the comparison. We set the transit depth at λ' to a plausible value such that $\beta = (F_p(\lambda')/F_*(\lambda')) \ll 1$ and the transit depth at λ , relative to the transit depth at λ' , is $\alpha = (F_p(\lambda)/F_p(\lambda'))$. $S_A(\lambda)$ can then be expressed in terms of α and β as,

$$S_A(\lambda) = G(t)F_*(\lambda) \left[1 + \alpha\beta \frac{F_*(\lambda')}{F_*(\lambda)} \right]. \quad (2)$$

During period B (star only), the measured signal, S_B , is $S_B(\lambda) = G(t)F_*(\lambda)$. The ratio of the two wavelengths during the A and B periods is $R_A = S_A(\lambda)/S_A(\lambda')$ and $R_B = S_B(\lambda)/S_B(\lambda')$. The advantage of taking the ratio is that the wavelength-independent gain term, $G(t)$, drops out. Appropriate substitution, and solving for α , yields,

$$\alpha = [R_A(1 + \beta) - R_B]/\beta \quad (3)$$

The observables are R_A and R_B , and α is the measure of the brightness of the planet at λ compared to the planet brightness at λ' . The results in figure 4 reflect a value for $\beta = 0.00225$. However, the results for the spectral slope are not strongly dependent on the assumed value for β , and we find a similar spectral shape for β values ranging from 0.001 to 0.004.

To estimate the magnitude of residual systematics, we have made a comparison (see Fig. 3) between two independent data sets (nod 1 in AOR 1 and nod 2 in AOR 2). We have taken the difference between averages of the normalized flux, $\langle R \rangle$, in the two data sets: $[\langle R(\text{nod1}, \text{AOR1}) \rangle - \langle R(\text{nod2}, \text{AOR2}) \rangle] / [0.5 * (\langle R(\text{nod1}, \text{AOR1}) \rangle + \langle R(\text{nod2}, \text{AOR2}) \rangle)]$ for the R_A (star+planet) and R_B (star only) cases. $\langle R_B \rangle$ difference is flat and very uniform as a function of wavelength, with a 1σ dispersion of 1.0×10^{-5} . This low value demonstrates the quality of the spectral flat fielding over the duration of the B period in the two data sets. The $\langle R_A \rangle$ difference curve shows considerably more noise with a dispersion of 200×10^{-5} , which is due to residual, wavelength-dependent, temporal drifts that were not corrected in the normalizing to a common wavelength, $12 \mu\text{m}$. The $\langle R_A \rangle$ curve suggests that the noise in an individual spectrum (normalized to $12 \mu\text{m}$) has a dispersion of roughly $200 \times 10^{-5} / \sqrt{2} \sim 140 \times 10^{-5}$, corresponding to an SNR of 700:1. The final normalized spectrum, which is the average of four independent spectra, would have a dispersion a factor of two smaller, $\delta R_A / R_A \sim 70 \times 10^{-5}$ or an SNR of 1400:1. It is on this basis that we claim an SNR ~ 4 relative to the transit signal of roughly 0.2%. A formal error analysis results in the uncertainties given in figure 4.

Method 2 - Pointing Correction: This approach begins with the assumption that changes in the measured source flux are due to telescope pointing errors. Pointing errors cause modulation of the measured flux because telescope motion perpendicular to the slit axis changes the position of the stellar image with respect to the spectrometer entrance slit, which changes the vignetting of the stellar image. Even small pointing errors change how the wings of the point spread function (PSF) are vignetted. Since the PSF size is proportional to wavelength, the measured flux changes due to pointing are wavelength dependent. Several sources of pointing error effect Spitzer including a periodic component caused by changes in the relation between the cryogenic telescope assembly and the spacecraft body (Bayward & Burgarolas 2004). We derived a pointing offset correction using the IRS cali-

brator source η Dor, which has been measured repeatedly and has also been observed with intentional slit displacements perpendicular to the slit axis. Using the Spitzer PSF, we modeled the effect of slit displacement on the measured spectral flux. Given the constraint that the spectrum of η Dor is constant, we fit the slit-scanned data with our PSF model to determine the relation between pointing error and measured flux as a function of wavelength. These results show that the typical pointing error associated with acquiring the source (± 0.25 arcsec in high-accuracy peak-up mode) can cause the measured source flux, $S(\lambda)$, to vary by $\sim 7\%$. The pointing offset correction space was explored by applying a pointing offset correction to each $S_i(\lambda)$ to obtain $F_i(\lambda, \theta)$ where θ is the pointing offset. To calibrate the HD 209458b data, we constructed all unique combinations of $\mathbf{R}(\mathbf{i}, \mathbf{j}) = F_i(\lambda, \theta)/F_j(\lambda, \theta)$ for the A and B portions of each nod separately, where i and j are individual measurements in the time series. We then iteratively searched the space of possible pointing offsets to determine the offset at each sample i , which resulted in most closely approximating $\mathbf{R}(\mathbf{i}, \mathbf{j}) = 1$. Figure 1 shows the results of the application of the pointing offset correction. Both the derivation of the pointing calibration and a description of how to apply it will be detailed in a forthcoming methods paper.

That the two spectral extraction procedures yield consistent results is encouraging (see Fig. 4). The largest pointing errors are static and occur during the initial peak-up and during the nod. Because the periodic pointing errors are relatively small, the change in the measured flux during a nod is, to first order, wavelength independent and the spectral flat field is a good approximation for the flux correction due to the initial pointing error. In detail, there are wavelength-dependent pointing effects, but these are smaller than the planetary signature within a nod.

4. Discussion

The relatively smooth character of the HD 209458b spectrum suggests the planet emission is dominated by purely thermal emission at these wavelengths. The spectral slope (using either method) is suggestive of thermal emission. From our analysis, we cannot distinguish the measured spectrum from a general, temperature-independent Rayleigh-Jeans spectrum, although we can rule out temperatures below 550 K and our results are consistent with previous results (Deming et al. 2004) which found $T \sim 1100$ K. The lack of spectral features rules out some classes of models and is consistent with models invoking clouds as the dominant source of thermal emission (Seager et al. 2005; Burrows et al. 2006; Fortney et al. 2005; Barman et al. 2005). Observations of HD 209458b by Charbonneau, et al. (2002) find relatively low levels of atmospheric Na while observations by Deming et al. (2005) place

relatively strong limits on the amount of CO. Those results imply that if clouds exist, they may lie at a relatively high elevation in the atmosphere of HD 209458b and cover most of the dayside; this would obscure most of the dayside atmospheric column. The dayside of the planet is strongly irradiated due to the short period orbit and tidal locking. Thus, if high-elevation clouds intercept a significant fraction of the incident radiation, it is possible that local heating of the atmosphere could result in a temperature inversion (Fortney et al. 2005; Burrows et al. 2006). We find the planet flux at $12\ \mu\text{m}$ is 0.40 ± 0.19 mJy and that normalised eclipse depth at $12\ \mu\text{m}$ is 0.0046 ± 0.0006 .

Our calibration achieves a dynamic range of $\sim 1400:1$ for the spectrum and $\sim 730:1$ per nod for the background. For comparison, the shot-noise-limited dynamic range at $9\ \mu\text{m}$ for these observations is $\sim 4,700:1$. The methods we have developed for calibration of the background and pointing errors represent a significant improvement in the state-of-the-art for IRS calibrations on bright objects. Of particular significance, we find the stability of the background to be sufficiently high that it should be possible to use the background as a stable reference for IRS spectroscopy of non-transiting exoplanets. Our calibration of the pointing error is adequate for the SNR needed for initial spectral characterization of HD 209458b. However, there is clearly scope for improvement, and we believe that carefully optimised observations could significantly increase the achieved dynamic range.

We thank the original PI team for the proposal and preparation of the AORs required to obtain these data. We also thank Drake Deming for several helpful conversations regarding the reduction of secondary eclipse data. We thank John Bayard for several helpful discussions concerning Spitzer pointing errors and Sara Seager for discussion regarding the possible role of clouds in exoplanet atmospheres.

REFERENCES

- Barman, T. S., Hauschildt, P. H., & Allard, F. 2005, *ApJ*, 632, 1132.
- Bayard, D. S., & Brugarolas, P. B. 2004, IOM, 3457-04-002.
- Beichman, C., et al. 2006, *ApJ*, 639, 1166.
- Bouwman, J., Lawson, W. A., Dominik, C., Feigelson, E. D., Henning, T., Tielens, A. G. G. M., & Waters, L. B. F. M. 2006, *ApJ*, 653, L57.
- Brown, T. M., Charbonneau, D., Gilliland, R. L., Noyes, R. W., & Burrows, A. 2001, *ApJ*, 522, 699.

- Bryden, G., et al. 2006, ApJ, 636, 1098.
- Burrows, A., Sudarsky, D., & Hubeny, I., 2006, ApJ, 650, 1140.
- Charbonneau, D., Brown, T. M., Latham, D. W., & Mayor, M. 2000, ApJ, 529, L45.
- Charbonneau, D., Brown, T. M., Noyes, R. W., & Gilliland, R. L. 2002, ApJ, 568, 377.
- Charbonneau, D., et al. 2005 ApJ626, 523.
- Deming, D., Seager, S., Richardson, L. J., & Harrington, J. 2005, Nature, 434, 740.
- Deming, D., Brown, T. M., Charbonneau, D., Harrington, J., & Richardson, J. L. 2005, ApJ, 622, 1149.
- Deming, D., Harrington, J., Seager, S., Richardson, L. J. 2006, ApJ, 644, 560.
- Fortney, J. J., Marley, M. S., Lodders, K., Saumon, D., & Freedman, R. 2005, ApJ, 627, L69.
- Harrington, J., Hansen, B. M., Luszca, S. H., Seager, S., Deming, D., Menou, K., Cho, J., & Richardson, J. L. 2006, astro-ph/06/10491.
- Houck, J. R. 2004, ApJS, 154, 18.
- Kurucz, R. L. 1992, IAU Symp. 149, Stellar Populations in Galaxies, 225.
- Richardson, L. J., Deming, D., Wiedemann, G., Goukenleuqe, C., Steyert, D., Harrington, J., & Esposito, L. W. 2003, ApJ, 584, 1053.
- Richardson, J. L., Harrington, J., Seager, S., & Deming, D. 2006, ApJ, 649, 1043.
- Seager, S., Richardson, L. J., Hansen, B. L. S., Menou, K., Cho, J. Y.-K., & Deming, D. 2005, ApJ632, 1122.
- Wittenmyer, R. A., et al. 2005, ApJ, 632, 1157.
- Werner, M. W., et al. 2004, ApJS, 154, 1.

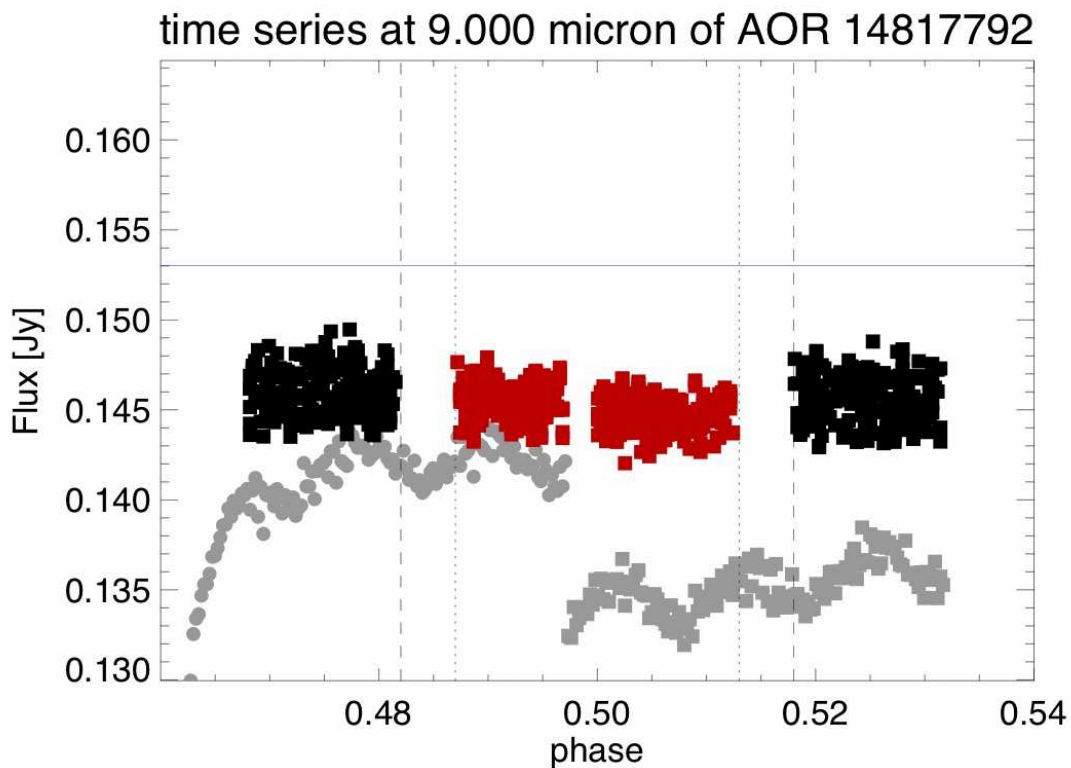


Fig. 1.— The $9\ \mu\text{m}$ flux time series for AOR 1 as a function of orbital phase. The measured data are shown in grey and the large discontinuity halfway through each data set corresponds to a nod; periodic changes and drifts also affect the time series measurements. The changes in measured flux are primarily due to telescope pointing errors which cause variable vignetting by the spectrometer entrance slit of the wings of the source point spread function. The black points (star+planet) and red point (star only) show the pointing corrected flux. The signature of the secondary eclipse is visible with the red points having a systematically lower flux value than the black points. The vertical dashed lines indicate the region of ingress/egress where the planet is partially obscured by the star.

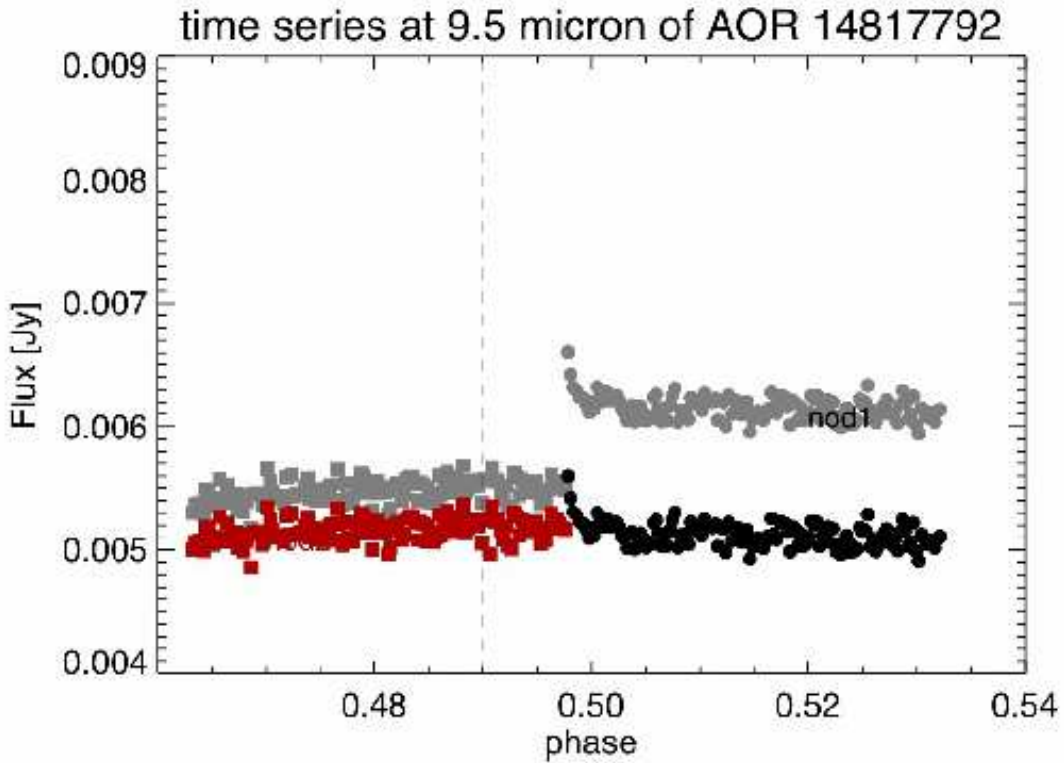


Fig. 2.— The off-source background before (grey) and after (red and black) correction for the source leakage. The asymmetric Spitzer PSF causes the source contribution (leakage) to be different for each nod and thus is responsible for the offset between the background level in the two nods.

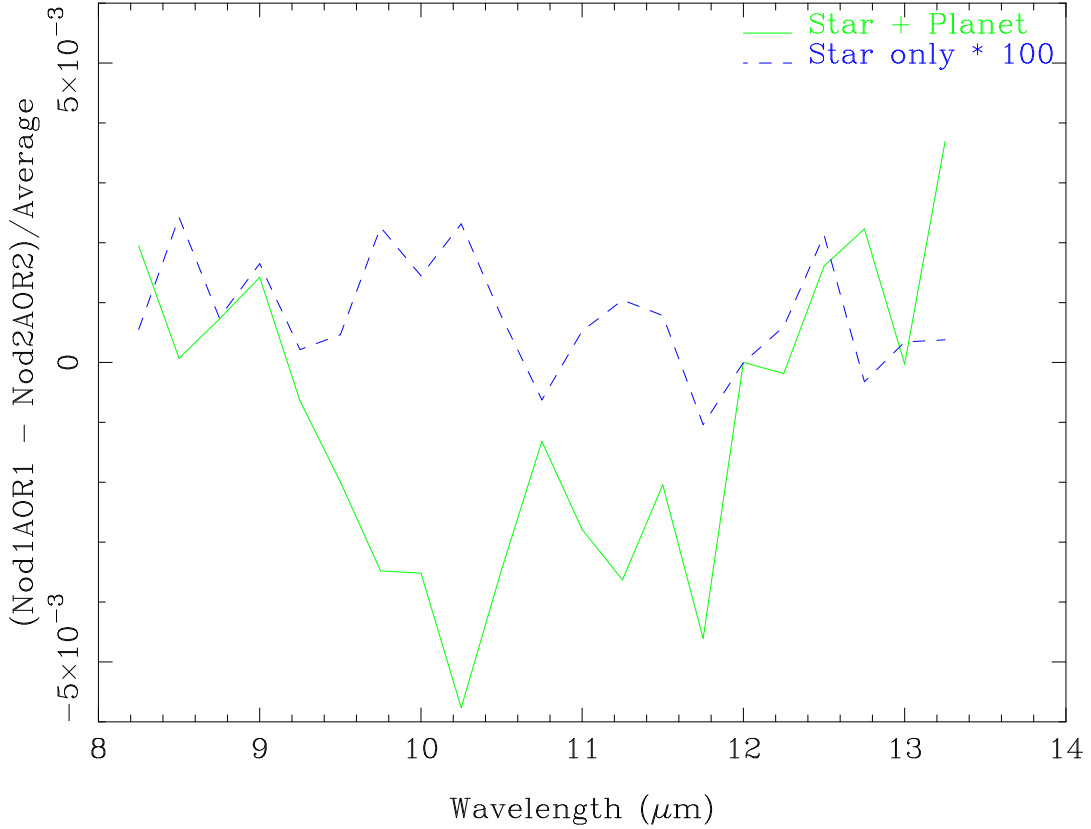


Fig. 3.— To estimate the residual systematic errors in method 1, we have plotted the difference between the average of the normalized flux for two independent datasets: $[\langle R(\text{Nod1}, \text{AOR1}) \rangle - \langle R(\text{Nod2}, \text{AOR2}) \rangle] / [0.5 * (\langle R(\text{Nod1}, \text{AOR1}) \rangle + \langle R(\text{Nod2}, \text{AOR2}) \rangle)]$ for the R_A (star+planet) and R_B (star only) cases. The R_B curve is flat as a function of wavelength with a 1 sigma dispersion of 1.0×10^{-5} and demonstrates the quality of the spectral flat fielding. The R_A curve shows considerably more noise with a dispersion of 200×10^{-5} which is due to residual, wavelength-dependent temporal drifts that were not corrected in the normalizing to the $12 \mu\text{m}$ flux.

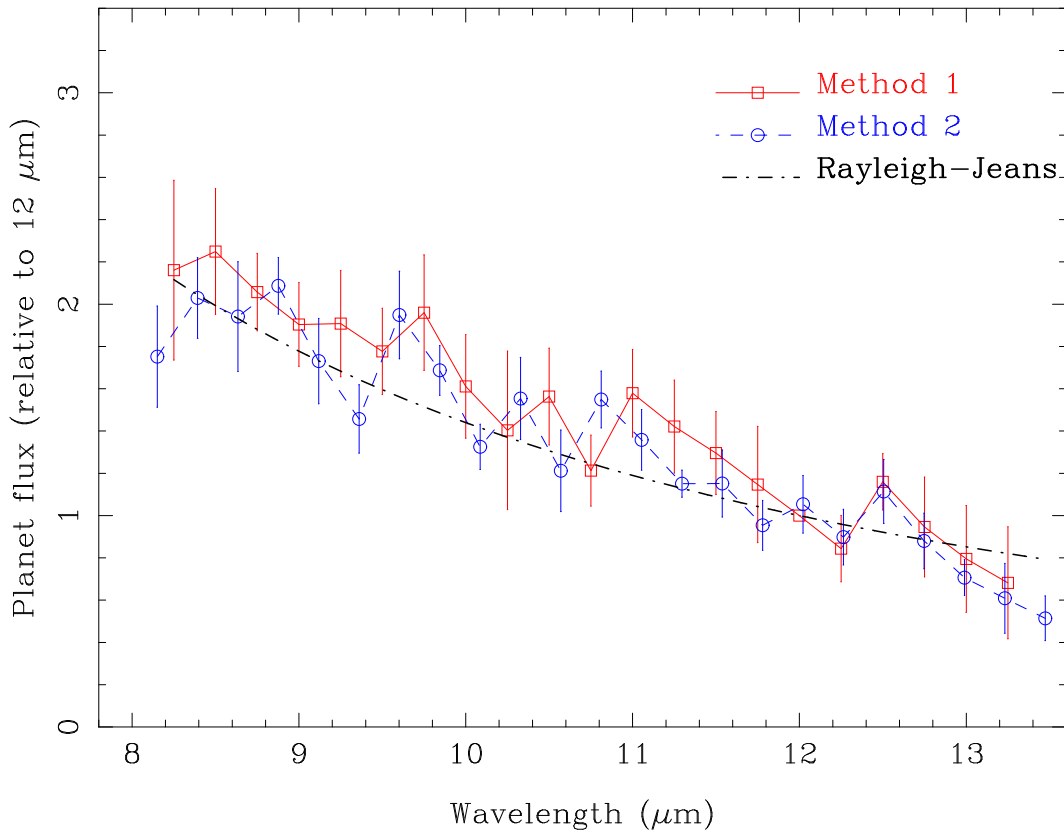


Fig. 4.— The mid-infrared spectrum of HD 209458b derived using two independent methods. For both cases, the spectrum has been normalised to the $12\ \mu\text{m}$ flux and scaled so that the average flux for both plots is identical. The first method (open circles) is a differential method and relies on correction based on a spectral flat field. The second method preserves information about the planet flux and relies on a correction for telescope pointing errors; the planet flux at $12\ \mu\text{m}$ is 0.4 ± 0.19 mJy. The smooth character of the exoplanet emission suggests it is largely thermal and it is most consistent with emission from clouds.

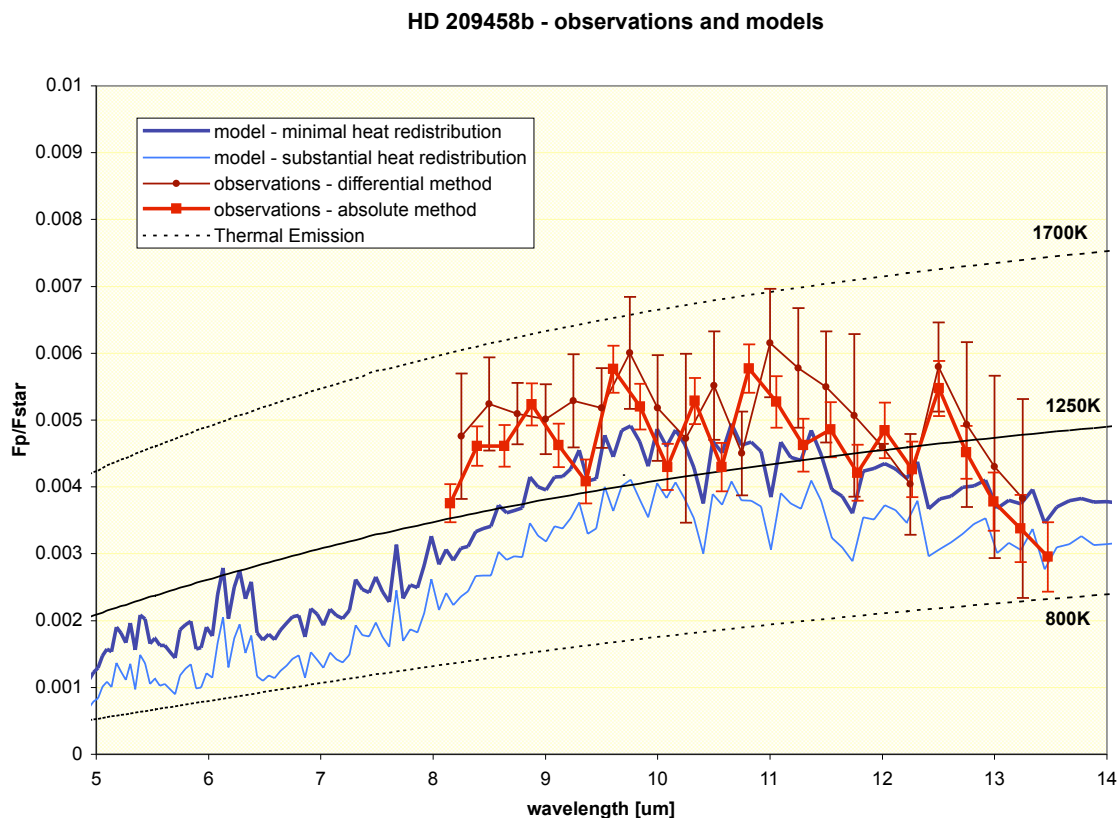


Fig. 5.— The two methods (absolute and differential) developed by our team for determining the mid-infrared spectrum of HD 209458b are plotted together with two models (Burrows et al. 2006) for the exoplanet emission. The agreement between the two methods for determining the spectra demonstrates the excellent control of instrument systematics achieved in our calibration. The departure of the measurement from the models in the 8 to 9 micron region of the spectrum is significant; we interpret this difference as a possible indication of the presence of high clouds. The figure clearly shows that Spitzer/IRS observations between 5 and 8 microns would be crucial for advancing our understanding of this object. Further, our analysis shows that significantly higher SNR could be obtained with IRS by observations designed to minimize instrument systematics.